

# Characterization of fine-grained montmorillonite fractions for preparing polymer-clay nanocomposites

VĚRA VALOVIČOVÁ<sup>1</sup>, SILVIA DOLINSKÁ<sup>2\*</sup>, LENKA VACULÍKOVÁ<sup>1</sup>, EVA PLEVOVÁ<sup>1</sup>,  
INGRID ZNAMENÁČKOVÁ<sup>2</sup> and ZUZANA DANKOVÁ<sup>3</sup>

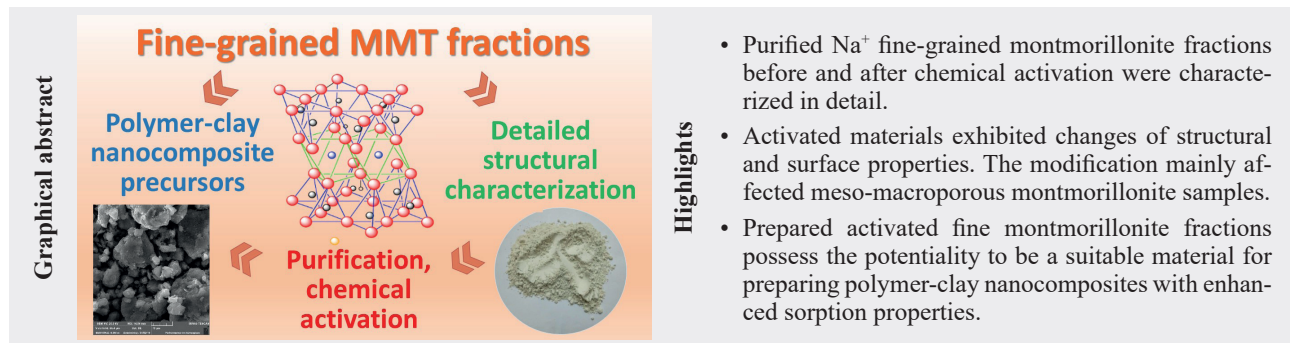
<sup>1</sup>Institute of Geonics of the Czech Academy of Sciences, Studentská 1768, CZ–708 00 Ostrava-Poruba,  
Czech Republic

<sup>2</sup>Slovak Academy of Sciences, Institute of Geotechnics, Watsonova 45, SK–040 01 Košice,  
Slovak Republic; \*sdolinska@saske.sk

<sup>3</sup>State Geological Institute of Dionýz Štúr, Department of Applied Technology of Raw Materials, Jesenského 8,  
SK–040 01 Košice, Slovak Republic

**Abstract:** Detailed structural characterization of clay minerals contributes to a better understanding of their behavior and physico-chemical properties, making it possible to fully exploit their potential for polymer-clay nanocomposite preparation and their future industrial applications. The object of this study was to characterize fine-grained fractions of four montmorillonite samples and compare them with untreated montmorillonite. The gained results confirmed that fine montmorillonite fractions would be more appropriate precursors for successive preparing of composite materials with sorption property enhancement, useable for environmental remediation.

**Key words:** montmorillonite, source clays activation, characterization



## 1 Introduction

Nanoclays are nanoparticles of layered silicates that can be used in the design and preparation procedure of polymer/clay nanocomposites (Ray & Okamoto, 2003). The integration of nanoclays into polymeric matrixes improves the physico-chemical and mechanical properties of polymers (Kanmani & Rhim, 2014; Gautam & Komal, 2019; Qin et al., 2021). Among the reasons for wide research of nanocomposite precursors founded on clay and layered silicates belong their easy availability as well as the fact that their intercalation chemistry was investigated for a long time (Ray & Okamoto, 2003; Pavlidou & Papaspyrides, 2008; Kanmani & Rhim, 2014). Advantages of nanoclays include high specific surface area, easy processability, good performance, and lower cost. Nanoclays used as a fillers of nanocomposites are usually in the form of 2-dimensional platelets with a thickness of ca. 1 nm and a length of several

micrometers (Ruitz & Van Meerbeek, 2006; Brantseva et al., 2018). A layered silicate montmorillonite (MMT) can be designated as one of the most commonly used nanoagents for preparing nanocomposites (de Azeredo, 2013). Its chemical general formula (without structural substitutions) is  $(OH)_4Si_8Al_4O_{20}\cdot nH_2O$  (Parekh & Rule, 2002). Generally, montmorillonite can be classified by the types of interlayer cations in montmorillonite into sodium and calcium montmorillonite. Calcium montmorillonite (CaMMT) has two H<sub>2</sub>O molecular layers in the interlayer whereas sodium montmorillonite (NaMMT) contains typically single layer of water molecules. Important properties of CaMMT associated with their use include especially high absorption capacity, bleaching ability and bonding strength, NaMMT is characterized by higher swelling and viscosity (Tombacz & Szekeres, 2004; Wiess & Kužvar, 2005; Murray, 2007; Shah, 2018; Hayakawa et al., 2019).

Many industries (engineering, petroleum discovery, recovery and refining, etc.) use the clay minerals due to their composition and structure (Wiess & Kužvar, 2005; Ruitz & Van Meerbeek, 2006; Murray, 2007). Particle size, layer charge, swelling capacity, surface area and surface chemistry belong to the important characteristics connecting with applications of clay minerals. Modification of clays has a significant effect on the structural properties – very often causing an improvement in their sorption capacities (Sanqin et al., 2014; Kotal & Bhowmick, 2015; Alves et al., 2017; Tomić et al., 2018; Guo et al., 2020). This further functionalization of clay minerals is possible through substituting the exchangeable cations with organic molecules (Abollino et al., 2003; Hong & Rhim, 2008), by pillaring (Bergaya et al., 2006) or acid activation (Komadel & Madejová, 2006). Another possibility may be a magnetic modification in which the layered silicates are coated with iron oxides (Mockovčiaková et al., 2010). Modified and functionalised nanoclays are widely used for remediating environmental contaminants (Abollino et al., 2003; Al-Degs et al., 2006; Guerra et al., 2013; Akpomie & Dawodu, 2014; Schütz et al., 2016; Abdellaoui et al., 2017; Uddin, 2017; Galamboš et al., 2012; Galamboš et al., 2013), they show promise as advanced sorbents or biodegradation enhancers (Biswas et al., 2019).

Clay minerals are also used as a catalysts, their activity has been demonstrated in a number of reactions. Last but not least, application of montmorillonite clays as green catalysts plays role in developing eco-friendly chemical processes (Kaur & Kishore, 2012). The catalytic properties of natural clays are enhanced by acid activation, which causes an increase in nitrogen surface area and adsorptive capacity of activated materials. The activation process can sometimes lead to the destruction of clay mineral structure as it removes Fe, Al and Mg cations from the octahedral layer. Generally, the clay minerals having a high octahedral magnesium or iron content leach more easily than such materials with high octahedral aluminium content. Moreover, the hydrophilic surface of swelling clay material can become organophilic through the exchange of inorganic cations (naturally occurring) with organocations. It caused the extension of the layers for access the non-polar molecules to the interlamellar space (Breen & Moronta, 2001).

This paper is aimed at detailed structural characterization of fine-grained MMT fractions for preparing polymer-clay nanocomposites. Natural montmorillonite clays can consist of fine-grained elements of clay minerals accompanied by crystals of various minerals including quartz, carbonates, feldspars and also metal oxides (Ruitz & Van Meerbeek, 2006). These impurities presented in the natural montmorillonite composition can negatively influence the adsorption characteristic of the future synthesized nanomaterials.

## 2 Materials and methods

### 2.1 Materials

The four montmorillonite samples (Tab. 1) used in this study were: SWy-2, SAz-2, STx-1b (from the Source Clays Repository, the Clay Minerals Society, USA) and Kunipia-F (from Kunimine Industries Co. Ltd., Japan). The SAz-2 and STx-1b samples contain calcium in the interlayer, the SWy-2 sample shows the presence of both  $\text{Na}^+$  and  $\text{Ca}^{2+}$  cations and Kunipia-F belongs to sodium type clay.  $\text{Na}_2\text{CO}_3$  was of analytical purity from Merck Ltd., Germany.

**Tab. 1**  
Overview of used montmorillonite samples.

Sample	Description	Locality	Impurities XRD <sup>a</sup>	Impurities FT-IR <sup>b</sup>
SAz-2	CaMMT	Arizona, USA	–	opal*
STx-1b	CaMMT	Texas, USA	opal	cristobalite
SWy-2	Ca, NaMMT	Wyoming, USA	mica, quartz	quartz (mica), carbonate*
Kunipia-F	NaMMT	Kunimine Co., Japan	mica, quartz	quartz (mica), carbonate*

Notes: <sup>a</sup>Detected by XRD analysis. <sup>b</sup>Detected by FT-IR spectroscopy analysis. \*The impurity occurs in traces.

The detailed study of these MMT standard samples by Infrared and Raman spectroscopy were performed by the authors Ritz and Vaculíková (Ritz et al., 2016; Vaculíková et al., 2019) in previous study. Some of the necessary information obtained from these analytical methods can be found in Tab. 1 and 2.

**Tab. 2**  
Major elemental composition of montmorillonitic clay samples.

Sample	CaO	$\text{Na}_2\text{O}$	$\text{SiO}_2$	$\text{Al}_2\text{O}_3$	MgO	$\text{Fe}_2\text{O}_3$	$\text{K}_2\text{O}$	$\text{TiO}_2$
SAz-2	2.42	< 0.05	51.5	14.8	5.0	1.4	0.2	0.2
STx-1b	1.6	0.2	65.4	12.6	2.6	1.0	0.2	0.2
SWy-2	1.5	1.4	61.2	17.8	2.5	3.7	0.6	0.1
Kunipia-F	0.4	3.0	58.5	19.0	3.0	1.8	0.1	0.2

The SWy-2, SAz-2, STx-1b and Kunipia-F samples in their natural form were first purified by sedimentation to eliminate inorganic mineral impurities. Clay fractions

with particle size below 5 µm were collected according to Stokes law, the sedimentation time was derived from the selected particle size. To improve the sorption properties of fine montmorillonites, their monoionic chemical activation was performed. The fractions of montmorillonite samples containing calcium in the interlayer were modified by the saturation with Na<sub>2</sub>CO<sub>3</sub>; SWy-2, SAz-2, STx-1b fine fractions were mixed with 0.5 M aqueous solution of Na<sub>2</sub>CO<sub>3</sub> by shaking for 24 h. After intensive mixing the mixture was separated by centrifugation. Sedimented Na-clay mineral fine fractions were rinsed repeatedly with distilled water. After that the fine clay productions were dried at 100°C for 24 h. The activated samples were labeled as NaSAz-2, NaSTx-1b and NaSWy-2.

## 2.2 Methods characterization

The X-ray powder diffraction (XRD) analysis was obtained by the X-ray diffractometer Bruker D8 Advance (40 kV, 40 mA), using CuK $\alpha$  radiation. For interpretation of the diffraction phases was used the Joint Committee for Powder Diffraction Data – International Centre for Diffraction Data (the JCPDS database).

Infrared spectra of montmorillonites were obtained using Fourier transform infrared (FT-IR) spectrometer Nicolet 6700. The configuration of FT-IR spectrometer and experimental conditions were as follows: middle infrared (MIR) region (4 000–400 cm<sup>-1</sup>): ETC EverGlo IR source, KBr beam splitter and DTGS KBr detector. For sample preparation was used KBr pressed disk technique: approximately 1 mg of sample and 200 mg dried KBr pressed under pressure into a transparent disc. For each sample, 64 scans were measured in the abs mode with a resolution of 4 cm<sup>-1</sup>.

Thermal curves were collected by simultaneous thermogravimetry and differential thermal analysis (TG/DTA) with thermal device Setsys Evolution 24, Setaram, France. Measurements were recorded under argon atmosphere with heating rate 10 °C·min<sup>-1</sup>, final temperature 1 200 °C and cca 15 mg of sample.

Textural properties of studied montmorillonites were determined by method of physical adsorption of nitrogen at -196 °C by NOVA 1 200e Surface Area & Pore Size Analyzer (Quantachrome Instruments, USA). The samples were degassed at 100 °C in a vacuum oven under a pressure lower than 2 Pa for 18 hours. The specific surface ( $S_{BET}$ ) was calculated from the adsorption isotherms following the BET (Brunauer, Emmett, Teller) method in the range of relative pressure 0.05–0.2. The volume of micropores

( $V_{micro}$ ) and the external surface ( $S_e$ ) were gained by use of the t-plot method analysis using the Harkins-Jura standard isotherm. The value of total pore volume ( $V_{tot}$ ) was estimated from the maximum adsorption at relative pressure close to saturation pressure. The total pore volume was derived from the nitrogen volume adsorbed at the relative pressure  $p/p_0 \rightarrow 1$ . The pore size distribution was determined using the BJH (Barrett, Joyner, Halenda) method from the desorption part of the isotherms.

The overview morphologies of the investigated samples were acquired by field emission scanning electron microscope TESCAN MIRA 3 FE SEM with an accelerating voltage of 20 kV. The sample particles were examined at magnifications of 5 000x.

## 3 Results

### 3.1 X-ray diffraction analysis

The X-ray diffraction analysis (XRD) shows the changes in a structure of fine-grained MMT fractions before and after their monoionic chemical activation (Fig. 1, Tab. 3).

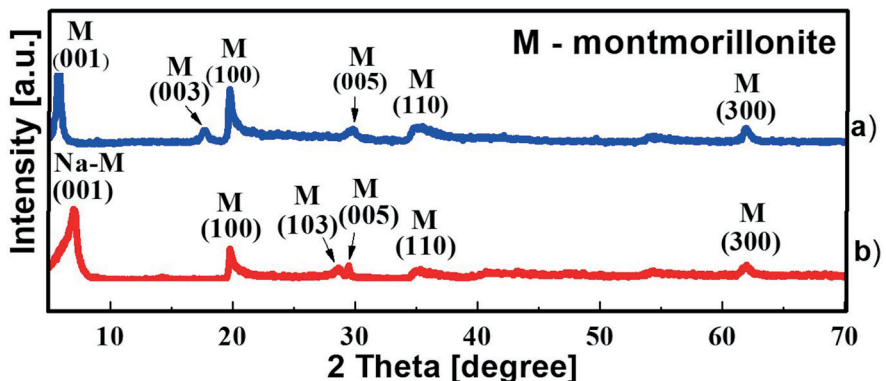


Fig. 1. XRD diffraction patterns of montmorillonite samples: a) CaMMT; b) NaMMT.

The basal reflections 001 in original samples with the interlayer space values (d) vary from 12.43 Å to 15.24 Å. It is caused by presence of exchangeable inorganic cations in the interlayer space of the samples. The SAz-2 sample shows the most intensive basal reflection 001 with the higher interlayer space value 15.24 Å which confirms the presence of Ca<sup>2+</sup> in the interlayer space (Iwasaki & Watanabe, 1988). The basal reflection 001 in sample STx-1b with the interlayer space of d(001) = 14.63 Å is characteristic for the presence of Ca<sup>2+</sup> in the interlayer (Önal et al., 2007). The diffractogram of SWy-2 shows that the basal reflection with interlayer space of d(001) = 13.55 Å was reduced in comparison to the Kunipia-F. This change is probably due to the presence both Na<sup>+</sup> and Ca<sup>2+</sup> in the interlayer space. The Kunipia-F is the sample with the interlayer space value of d(001) = 12.43 Å, which

**Tab. 3**

Interlayer space values of original and activated fine montmorillonite fractions.

Sample	Description	d(001) [Å]	Activated sample	d(001) [Å]
SAz-2	CaMMT	15.24	NaSAz-2	12.83
STx-1b	CaMMT	14.63	NaSTx-1b	12.08
SWy-2	Ca,NaMMT	13.55	NaSWy-2	11.92
Kunipia-F	NaMMT	12.43	–	–

**Tab. 4**

Fundamental vibration frequencies of original montmorillonite samples.

Assignment	MMT SWy-2	MMT STx-1b	MMT SAz-2	MMT Kunipia-F
OH stretching of structural hydroxyl groups	3 627	3 624	3 621	3 626
OH stretching of water	3 427	3 429	3 425	3 440
OH deformation of water	1 636	1 636	1 637	1 638
Si-O of quartz	1 170	–	–	–
Perpendicular Si-O stretching	1 120	1 089	1 091	–
In plane Si-O-Si stretching	1 048	1 042	1 032	1 041
Al-Al-OH deformation	917	916	915	915
Al-Fe-OH deformation	884	–	–	–
Al-Mg-OH deformation	848	845	842	844
Si-O of quartz	798	–	–	798
Si-O of cristobalite	–	794	–	–
Si-O of silica (opal)	–	–	789	–
Si-O of quartz	779	–	–	779
Si-O of quartz	695	–	–	695
Coupled Al-O and Si-O, out-of-plane and Si-O of cristobalite	–	627	–	–
Coupled Al-O and Si-O, out-of-plane	622	–	622	622
Al-O-Si bending	524	521	519	522
Si-O-Si bending	467	469	466	467

is typical for the occupation of the interlayer space by calcium cations (Önal et al., 2007). The effect of chemical activation can be observed by comparison of MMT basal reflections 001. The shift of d(001) MMT reflection (Fig. 1, Tab. 3) to the right on the axis x for activated samples shows to the ion exchange in the interlayer space ( $\text{Ca}^+$  replaced by  $\text{Na}^+$ ).

### 3.2 Fourier transform infrared spectroscopy

The absorption spectra of the original montmorillonite forms obtained by the KBr-pressed technique are shown in Fig. 2. The absorption bands observed in these spectra are described in detail in Tab. 4. Individual types of montmorillonites differ not only in the type of mineral admixtures, but also in their chemical composition. It is evident, that the SAz-2 is a nearly pure specimen. Only slight shoulder occurring at  $789 \text{ cm}^{-1}$  indicates traces of amorphous silica. The quartz admixture was confirmed by doublet of bands at  $798$  and  $779 \text{ cm}^{-1}$  in SWy-2 and Kunipia-F. Sample STx-1b contains only cristobalite ( $794 \text{ cm}^{-1}$ ). The absorption band located at  $884 \text{ cm}^{-1}$  in sample SWy-2 demonstrates the presence of Fe in the octahedral structure of this clay mineral. After treatment of the mineral samples with a natrifying agent, typical carbonate bands ( $1 430$  and  $880 \text{ cm}^{-1}$ ) appear in all IR spectra of used montmorillonites. Simultaneously, the position of the band corresponding to the vibrations of the surface-bound water molecules changes, the band shifts to higher wavenumbers ( $3 445 \text{ cm}^{-1}$ ).

### 3.3 Thermal analysis

The samples of fine-grained montmorillonite fractions as well as the samples of their activated sodium forms were measured by TG/DTA to get an overview of their thermal behaviour. The studied samples exhibit the same trend as shown in the Fig. 3. The thermal curves of montmorillonite samples generally show two temperature intervals. The first interval ranges from  $100$  to  $300^\circ\text{C}$  and involves the release of adsorbed water from the interlayer. The second interval ranges from  $500$  to  $1 100^\circ\text{C}$  and involves the release of hydroxyl groups and subsequent phase

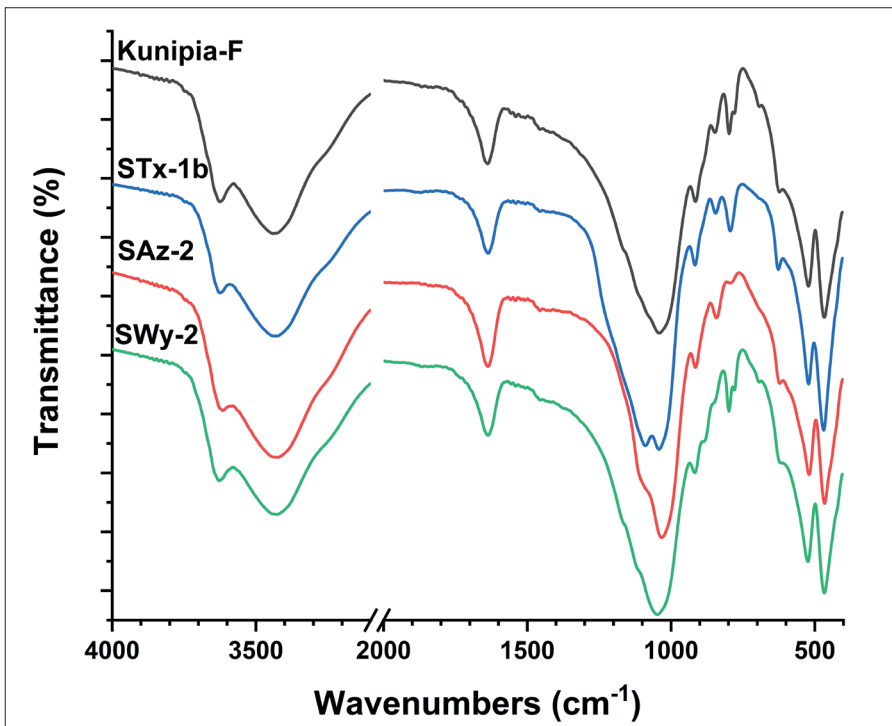


Fig. 2. FTIR spectra of original montmorillonite forms.

transformations. The temperatures, shapes and intensities of the endotherm peak in lower temperature interval are related to cations present in the sample (Hatakeyama & Liu, 1998). The doubled peak associated with loss of adsorbed water is connected to Ca-montmorillonite form, whereas after activation process there was obtained only one stage peak typical for Na-montmorillonite form (Blažek, 1974). Also the character of DTA curves for modified samples slightly differed in contrast to origin minerals. Moreover the temperature of phase transformation for STx-1b sample increased, but for SWy-2 and SAz-2 no phase transformation was observed.

### 3.3 Textural properties

The textural properties of MMT samples (SWy-2, SAz-2, STx-1b, Kunipia-F) and their natrified forms (NaSWy-2, NaSAz-2, NaSTx-1b) were studied by comparison their adsorption and desorption isotherms. The measured isotherms of all as-obtained MMT samples showed the hysteresis loop between the adsorption and desorption branches of isotherms. The hysteresis loop is generally related with the capillary condensation in mesopores, therefore their presence in the structure of studied samples is predicted. Adsorption isotherms of SWy-2, SAz-2 and Kunipia-F are very similar, slow increase of adsorbed gas volume in the whole range of relative pressure

with sharp increase at  $p/p_0 \approx 0.95$ , associated with the presence of larger pores, macropores, Fig. 4. For the sample Kunipia-F more regular increase of adsorbed gas volume with increasing relative pressure can be detected. The hysteresis loops of SWy-2, STx-1b and Kunipia-F as-obtained MMT samples correspond with Type H3, which relates with the presence of slit-like shape pores typical for aluminosilicate materials. The loop of SAz-2 sample is Type H4 also associated with presence of slit-like shape pores, but the initial part of the isotherm is connected with the presence of micropores, what was also confirmed from the processing of measured data by BET method, Tab. 5.

For the SAz-2 sample the BET isotherm exhibited the convex shape with the negative intercept indicating the occurrence

of higher volume of micropores. Based on negative value of intercept and  $C_{BET}$  constant acquired from the mathematical model (Tab. 5), the value of specific surface area is not of real physical significance. The BET method is suitable for mesoporous to macroporous materials (pores size bigger than 2 nm). For microporous samples should be employed data evaluations from other technique than BET. Therefore, allowing apparatus options, the texture of sample was gained applying the *t*-plot method using the

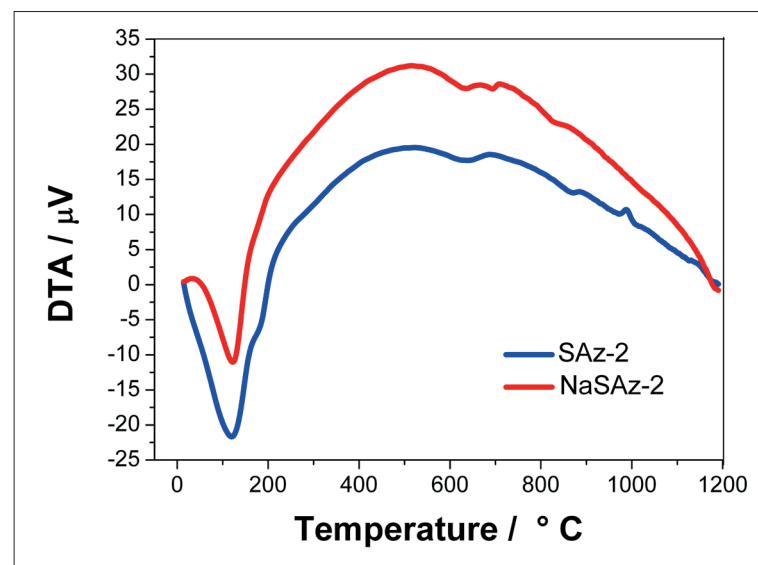


Fig. 3. DTA curves of CaMMT and NaMMT.

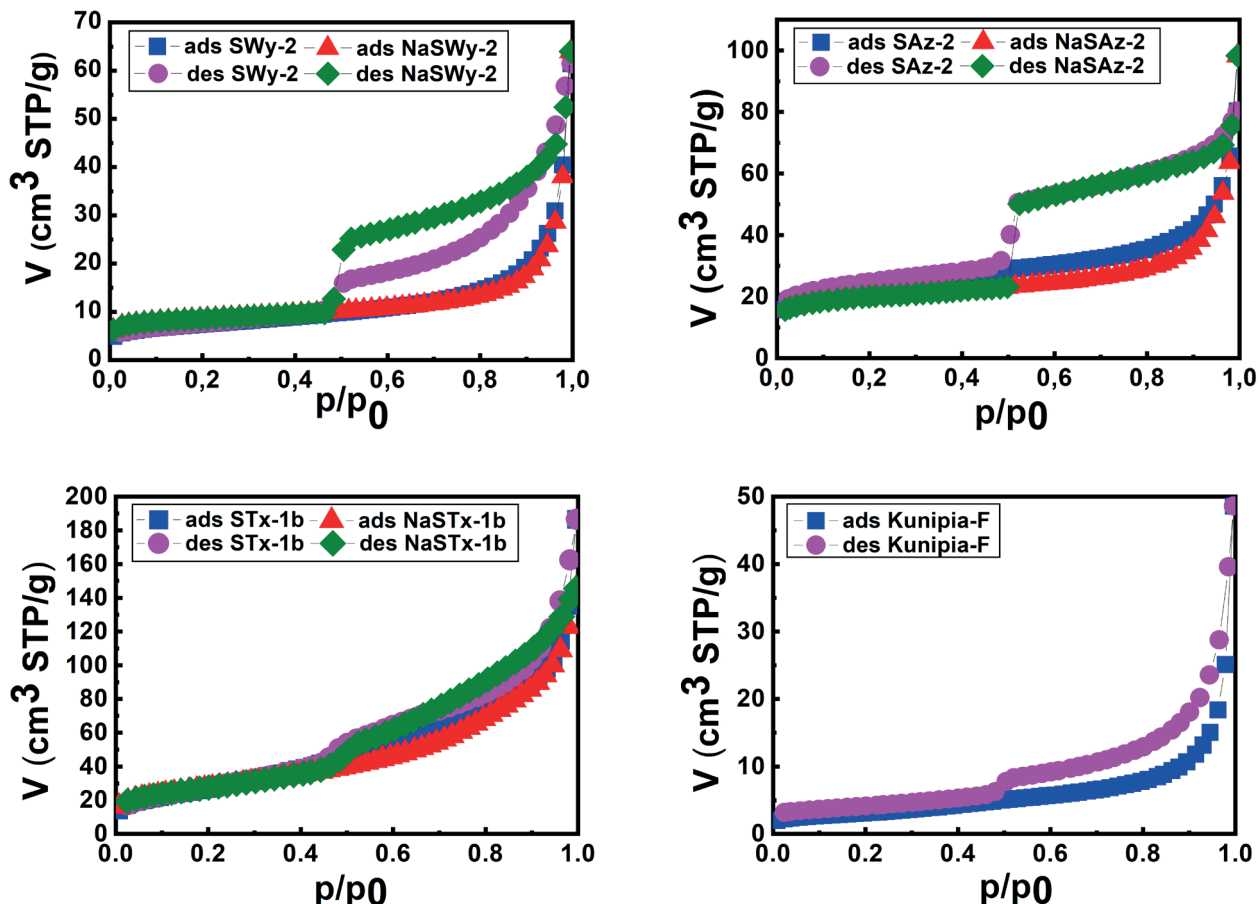


Fig. 4. Low temperature nitrogen adsorption – desorption isotherms of studied MMT samples.

Harkins-Jura isotherm. That permits to define the micropore volume and external surface area plus specific surface area of mesopores. While the STx-1b and Kunipia-F samples do not contain micropores, for the SAz-2 sample relative high volume of them was calculated. From the as-obtained MMT samples, the highest value of specific surface area was obtained for the STx-1b sample.

Modification of as-obtained montmorillonites did not change the shape of their isotherms significantly. The hysteresis loop got wider for all studied samples, Fig. 4. While for the SWy-2 and STx-1b samples similar gas volume was adsorbed at low relative pressure, for the SAz-2 sample slight decrease can be observed. For the SAz-2 sample the modification did not influence the textural properties as in case of other studied MMT samples. This sample was strongly microporous comparing with other studied materials and after the modification the volume of micropores only slightly increased. In case of NaSWy-2 sample more than twice higher value of micropore volume was obtained. Increase from the zero value up to significant value of  $0.004 \text{ cm}^3 \text{ STP/g}$  (STP – standard temperature and pressure,  $t = 0^\circ\text{C}$ ,  $p = 101.325 \text{ kPa}$ ) was detected for the

NaSTx-1b sample. For all samples, increase of micropore volume relates with the decrease in value of external surface area, Tab. 5.

The changes in textural properties of the as-obtained MMT samples after their modification can be observed also from the differential pore size distribution curves derived from the desorption branches of isotherms (Fig. 5).

The SWy-2 sample showed wider distribution in the range from  $4.3 \text{ nm}$  to  $44.7 \text{ nm}$  with maximum  $R_{\max} = 9.8 \text{ nm}$  (pore radius) what corresponds with the presence of meso- and macropores. The sharp maximum of pore radius at  $R \approx 1.9 \text{ nm}$  correlates with the jump on the desorption isotherm, as called forced close of hysteresis loop and does not correspond with real pores. This maximum can be observed for all studied samples, therefore it was not regarded as significant data and the y axis of graphs were customized to better illustrate the differences between the curves. After the modification the distribution curve did not show significant maximum, but also the volume of meso- and macropores decreased. The sample SAz-2 and NaSAz-2 have very similar distribution curves, slight difference can be observed only in the range of large

mesopores and macropores what can be associated with the lower value of adsorbed gas volume on the adsorption isotherm discussed above. As was mentioned, the SAz-2 sample was more microporous and the modification did not influence its textural properties significantly. Therefore, almost similar run of distribution curves was obtained for these studied samples. The STx-1b as-obtained sample did not contain micropores. It was mainly meso-macroporous, with higher content of larger mesopores ( $R_{\max} = 21.6$  nm). After the sample modification,

the shift of the distribution curve to left to the values of lower mesopores was observed ( $R_{\max} = 3.05$  nm). This fact corresponds with the decrease of its value of total pore volume. The as-obtained Kunipia-F sample showed wide distribution from 3.03 nm to 143.3 nm with two maxima  $R_{\max 1} = 15.7$  nm and  $R_{\max 2} = 46.5$  nm, what confirmed its

**Tab. 5**  
Textural parameters of MMT samples.

Sample	$S_{\text{BET}}$ [ $\text{m}^2/\text{g}$ ]	C const.	$V_{\text{tot}}$ [ $\text{cm}^3/\text{g}$ ]	$S_t$ [ $\text{m}^2/\text{g}$ ]	$V_{\text{micro}}$ [ $\text{cm}^3/\text{g}$ ]
SWy-2	26.2	1 662.0	0.095 04	17.6	0.003 82
NaSWy-2	29.6	-2 101.9	0.098 91	11.9	0.008 12
SAz-2	84.4	-1 031.0	0.124 30	48.8	0.015 94
NaSAz-2	69.3	-209.3	0.152 00	32.7	0.016 72
STx-1b	99.4	73.0	0.288 40	99.4	0.000 00
NaSTx-1b	97.2	149.3	0.224 80	86.3	0.004 47
Kunipia-F	11.1	170.5	0.075 15	9.5	0.000 67

predominantly mesoporous character with small value of specific surface area.

### 3.4 Scanning electron microscopy

Montmorillonite samples (MMT) were characterized by particles assembled into aggregates up to a few tens

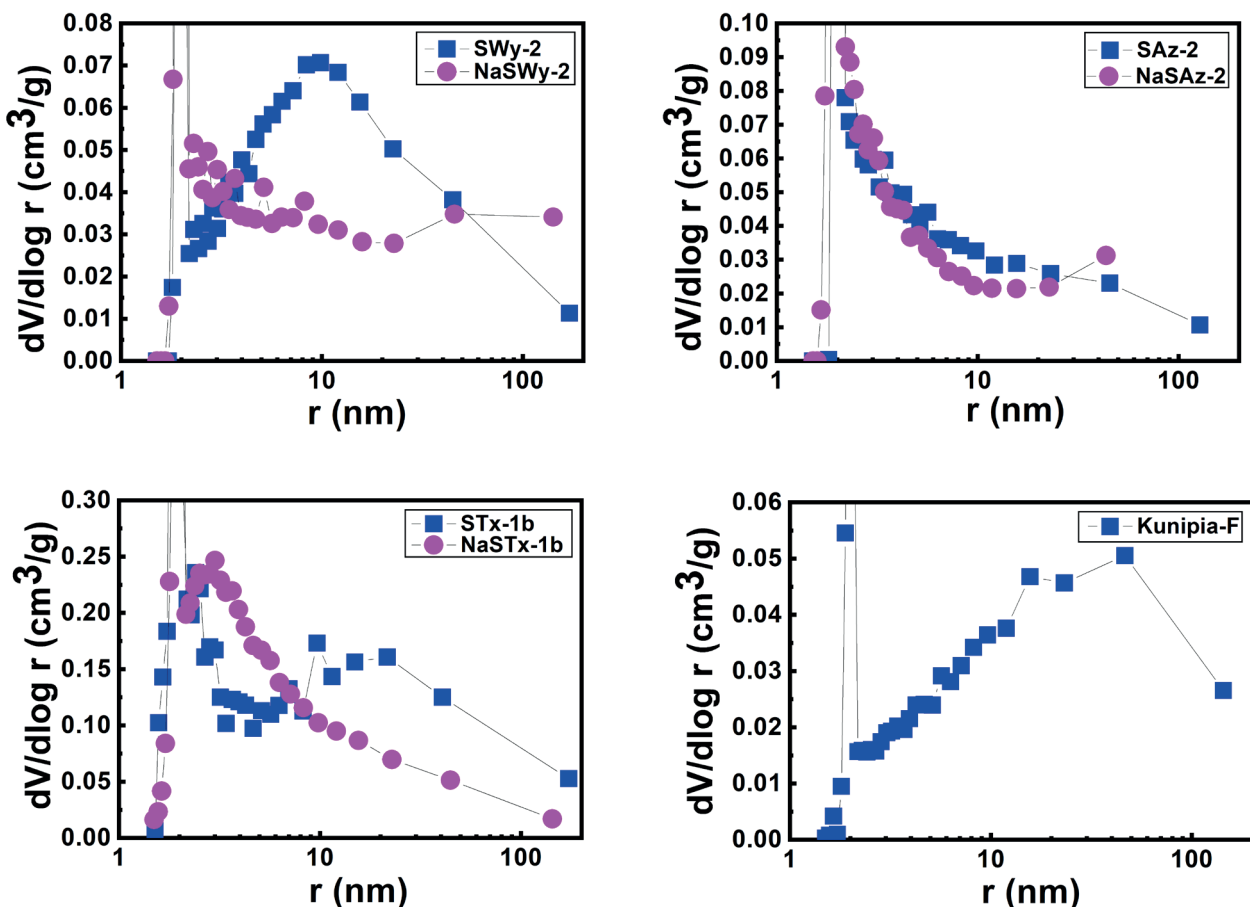
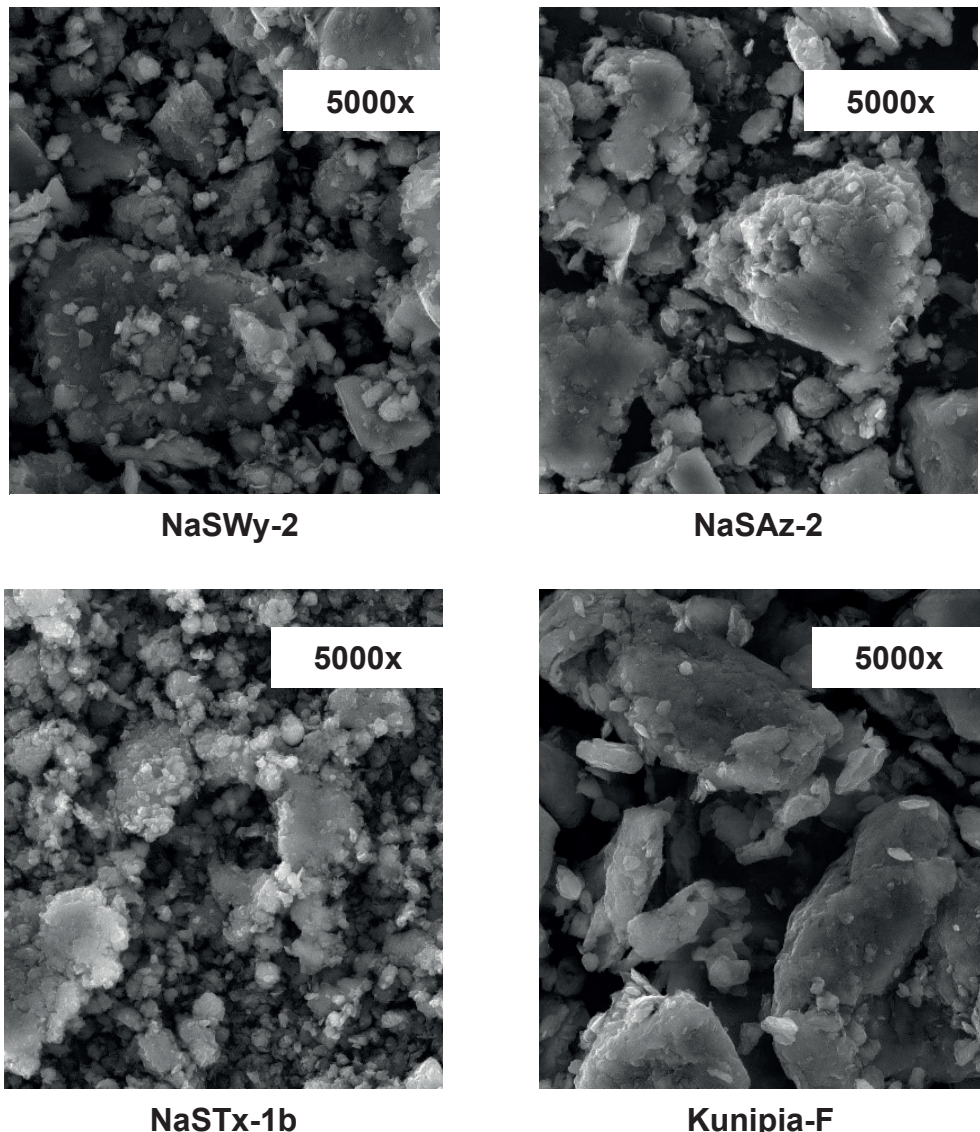


Fig. 5. Differential pore size distribution curves of studied MMT samples.



**Fig. 6.** SEM images of MMT samples – magnification 5 000x.

of  $\mu\text{m}$ . The montmorillonite natrification had a dispersing effect on montmorillonite which meant grain refinement (Fig. 6). The bonds in the structure of montmorillonite are mainly influenced by the presence of water molecules. Water absorption is directly related to the presence of the two most common  $\text{Na}^+$  and  $\text{Ca}^{2+}$  cations in the interlayer space of the MMT structure. Divalent  $\text{Ca}^{2+}$  cations keep the structural layers more stable and compact than their monovalent ( $\text{Na}^+$ ) competitors. Upon entering  $\text{Na}^+$  cations into the structure of smectite (montmorillonite), weaker bonds within the structural layers allow water molecules (but also other foreign cations or molecules) easier access to the layered structure. Hydration with water molecules leads to the expansion of the interlayer space immediately upon contact with water. A radical increase of the interlayer volume (up to 10 times) will affect the cation exchange

capacity of the montmorillonite (Kawatra & Ripke, 2003). In addition, monovalent  $\text{Na}^+$  cations cannot compensate for the negative target charge of the phyllosilicate, as the presently ordered divalent  $\text{Ca}^{2+}$  cations.

This results in the structure being refined by increasing the repulsive forces between the montmorillonite particles. This phenomenon, together with the increase in volume, leads to an increase in the specific surface area and to changes in the adsorption properties of montmorillonite (Fig. 6).

#### 4 Conclusion

In this study, the detailed characterization of fine-grained fractions of the montmorillonites samples SWy-2, SAz-2, STx-1b and Kunipia-F (in their natural state and after modification) was performed. The XRD analysis

confirmed montmorillonite as dominant mineral phase and demonstrated the structural changes of purified activated samples. The above mentioned changes affected the movement of montmorillonite main (001) reflection to the right on x axis. This phenomenon was caused by cation exchange between  $\text{Ca}^{2+}$  and  $\text{Na}^+$  from interlayer space of montmorillonite structure.

The absorption bands observed in the IR spectra of the original montmorillonite forms were described in detail. After chemical activation, typical carbonate bands appear in all IR spectra of used montmorillonites. Simultaneously, the position of the band corresponding to the vibrations of the surface-bound water molecules changes, the band shifts to higher wavenumbers.

Thermal stability was determined for both fine-grained montmorillonite fractions and the samples of their activated sodium forms. Studied samples exhibit the same trend. The doubled peak on DTA curve associated with loss of adsorbed water is connected to Ca-montmorillonite form, whereas after activation process there was obtained only one stage peak typical for Na-montmorillonite form.

Based on the obtained data it can be concluded that modification influenced the structural and porous properties of SWy-2 and STx-1b samples (meso-macroporous samples). For microporous montmorillonites (SAz-2) such kind of treatment has not significant effect.

The activation of MMT samples with sodium led to a smaller grain sizes caused by the dispersive effect of sodium cations on the montmorillonite morphology seen on SEM.

These obtained results indicate that prepared activated fine montmorillonite fractions possess the potentiality to be a suitable material for preparing polymer-clay nanocomposites with enhanced sorptive properties usable for environmental remediation.

### Acknowledgement

The authors would like to thank the Czech Academy of Sciences and the Slovak Academy of Sciences for supporting this study (Mobility Plus Project, project ID number SAV-AV ČR-21-08). This work was also supported by the Slovak Grant Agency for Science VEGA grant No. 2/0167/21. This work was supported by the Slovak Research and Development Agency under the contract No. APVV-19-0302. Authors are grateful to Alexandra Bekényiová and one anonymous reviewer for inspiring suggestions improving primary manuscript.

### References

- ABDELLAOUI, Y., OLGUÍN, M. T., ABATAL, M., ALI, B., MÉNDEZ, S. E. D. & SANTIAGO, A. A., 2017: Comparison of the divalent heavy metals (Pb, Cu and Cd) adsorption behavior by montmorillonite-KSF and their calcium-and sodium-forms. *Superlatt. Microstruct.*, 127, 165–175.
- ABOLLINO, O., ACETO, M., MALANDRINO, M., SARZANINI, C. & MENTASTI, E., 2003: Adsorption of heavy metals on Na-montmorillonite. Effect of pH and organic substances. *Water Res.*, 37, 7, 1619–1627.
- AKPOMIE, K. G. & DAWODU, F. A., 2014: Efficient abstraction of nickel (II) and manganese (II) ions from solution onto an alkaline-modified montmorillonite. *J. Taibah Univ. Sci.*, 8, 4, 343–356.
- AL-DEGS, Y. S., EL-BARGHOUTHI, M. I., ISSA, A. A., KHRAISHEH, M. A. & WALKER, G. M., 2006: Sorption of Zn (II), Pb (II), and Co (II) using natural sorbents: equilibrium and kinetic studies. *Water Res.*, 40, 14, 2645–2658.
- ALVES, J. L., ROSA, P. D. T. V. & MORALES, A. R., 2017: Evaluation of organic modification of montmorillonite with ionic and nonionic surfactants. *Appl. Clay Sci.*, 150, 23–33.
- BERGAYA, F., AOUAD, A. & MANDALIA, T., 2006: Pillared Clays and Clay Minerals. In: Bergaya, F., Theng, B. K. G. & Lagaly, G. (Eds.): *Handbook Clay Sci.*, Elsevier, Amsterdam, 1, 393–421,
- BISWAS, B., WARR, L. N., HILDER, E. F., GOSWAMI, N., RAHMAN, M. M., CHURCHMAN, J. G., VASILEV, K., PAN, G. & NAIDU, R., 2019: Biocompatible functionalisation of nanoclays for improved environmental remediation. *Chem. Soc. Rev.*, 48, 14, 3740–3770.
- BLAŽEK, A., 1974: Book of Thermal Analysis. Prague, SNTL.
- BRANTSEVA, T. V., ANTONOV, S. V. & GORBUNOVA, I. Y., 2018: Adhesion properties of the nanocomposites filled with aluminosilicates and factors affecting them: A review. *Int. J. Adhesion Adhesives*, 82, 263–281.
- BREEN, C. & MORONTA, A. J., 2001: Influence of exchange cation and layer charge on the isomerization of a-pinene over SWy-2, SAz-1 and Sap-Ca. *Clay Miner.*, 36, 467–472.
- DE AZEREDO, H. M., 2013: Antimicrobial nanostructures in food packaging. *Trends Food Sci. Technol.*, 30, 1, 56–69.
- GALAMBOŠ, M., DAŇO, M., ROSSKOPFOVÁ, O., ŠERŠEŇ, F., KUPČÁKOVÁ, J., ADAMCOVÁ, R. & RAJEC, P., 2012: Effect of gamma-irradiation on adsorption properties of Slovak bentonites. *J. Radioanal. Nucl. Chem.*, 292, 481–492.
- GALAMBOŠ, M., KRAJNÁK, A., ROSSKOPFOVÁ, O., VIGLAŠOVÁ, E., ADAMCOVÁ, R. & RAJEC, P., 2013: Adsorption equilibrium and kinetic studies of strontium on Mg-bentonite, Fe-bentonite and illite/smectite. *J. Radioanal. Nucl. Chem.*, 298, 1031–1040.
- GAUTAM, A. & KOMAL, P., 2019: Synthesis of montmorillonite clay/poly(vinyl alcohol) nanocomposites and their mechanical properties. *J. Nanosci. Nanotechnol.*, 19, 12, 8071–8077.
- GUO, Y. X., LIU, J. H., GATES, W. P. & ZHOU, Ch. H., 2020: Organo-modification of montmorillonite. *Clays Clay Mine.*, 68, 6, 601–622.
- GUERRA, D. J. L., MELLO, I., RESENDE, R. & SILVA, R., 2013: Application as absorbents of natural and functionalized Brazilian bentonite in  $\text{Pb}^{2+}$  adsorption: Equilibrium, kinetic, pH, and thermodynamic effects. *Water Res. Industry*, 4, 32–50.
- HATAKEYAMA, T. & LIU, Z., 1998: Handbook of Thermal Analysis. New York, Wiley.

- HAYAKAWA, T., OYA, M., MINASE, M., FUJITA, K. I., TEEPAKAKORN, A. P. & OGAWA, M., 2019: Preparation of sodium-type bentonite with useful swelling property by a mechanochemical reaction from a weathered bentonite. *Appl. Clay Sci.*, 175, 124–129.
- HONG, S. I. & RHIM, J. W., 2008: Antimicrobial activity of organically modified nano-clays. *J. Nanosci. Nanotechnol.*, 8, 11, 5818–5824.
- IWASAKI, T. & WATANABE, T., 1988: Distribution of Ca and Na ions in dioctahedral smectites and interstratified dioctahedral mica/smectites. *Clays Clay Mine.*, 36, 1, 73–82.
- KANMANI, P. & RHIM, J. W., 2014: Physical, mechanical and antimicrobial properties of gelatin based active nanocomposite films containing AgNPs and nanoclay. *Food Hydrocolloids*, 35, 644–652.
- KAUR, N. & KISHORE, D., 2012: Montmorillonite: An efficient, heterogeneous and green catalyst for organic synthesis. *J. Chem. Pharmaceut. Res.*, 4, 2, 991–1015.
- KOMADEL, P. & MADEJOVÁ, J., 2006: Acid activation of clay minerals. In: Bergaya, F., Theng, B. K. G. & Lagaly, G. (Eds.): *Handbook of Clay Science, Amsterdam, Elsevier*, 1, 263–287.
- KOTAL, M. & BHOWMICK, A. K., 2015: Polymer nanocomposites from modified clays: Recent advances and challenges. *Progress Polymer Sci.*, 51, 127–187.
- KAWATRA, S. K. & RIPKE, S. J., 2003: Laboratory studies for improving green ball strength in bentonite-bonded magnetite concentrate pellets. *Int. J. Mineral Process.*, 72, 1–4, 429–441.
- MOCKOVČIAKOVÁ, A., OROLÍNOVÁ, Z. & Škvarla, J., 2010: Enhancement of the bentonite sorption properties. *J. Hazard. Mater.*, 180, 1–3, 274–281.
- MURRAY, H. H., 2007: *Applied Clay Mineralogy. Amsterdam – Oxford, Elsevier*.
- ÖNAL, M., KAHRAMAN, S. & SARIKAYA, Y., 2007: Differentiation of  $\alpha$ -cristobalite from opals in bentonites from Turkey. *Appl. Clay Sci.*, 35, 1–2, 25–30.
- PAREKH, S. B. & RULE, A. U., 2002: Teaching Clay Science, In: Rule, A. U. & Guggenheim, S. (Eds.): *Clay Mineral Soc., Aurora*, 11, 22.
- PAVLIDOU, S. & PAPASPYRIDES, C. D., 2008: A review on polymer-layered silicate nanocomposites. *Progress Polymer Sci.*, 33, 111–1198.
- QIN, Z., PENG, T., SUN, H., ZENG, L. & ZHOU, C., 2021: Effect of montmorillonite layer charge on the thermal stability of bentonite. *Clays Clay Miner.*, 69, 328–338.
- RAY, S. S. & OKAMOTO, M., 2003: Polymer/layered silicate nanocomposites: a review from preparation to processing. *Progress Polymer Sci.*, 28, 11, 1539–1641.
- RITZ, M., VACULÍKOVÁ, L., KUPKOVÁ, J., PLEVOVÁ, E. & BARTOŇOVÁ, L., 2016: Different level of fluorescence in Raman spectra of montmorillonites. *Vibrational Spectrosc.*, 84, 7–15.
- RUITZ, E. & VAN MEERBEEK, A., 2006: Clay Mineral and Organoclay – Polymer Nanocomposites. In: Bergaya, F., Theng, B. K. G. & Lagaly, G. (Eds.): *Handbook of Clay Science, Amsterdam, Elsevier*, 1, 583–621.
- SANQIN, W., ZEPENG, Z., YUNHUA, W., LIBING, L. & JIANSHENG, Z., 2014: Influence of montmorillonites exchange capacity on the basal spacing of cation-anion organo-montmorillonites. *Mater. Res. Bull.*, 59, 59–64.
- SCHÜTZ, T., DOLINSKÁ, S., HUDEC, P., MOCKOVČIAKOVÁ, A. & ZNAMENÁČKOVÁ, I., 2016: Cadmium adsorption on manganese modified bentonite and bentonite-quartz sand blend. *Int. J. Miner. Process.*, 150, 32–38.
- SHAH, L. A., 2018: Effect of  $\text{Na}_2\text{CO}_3$  activation and sedimentation on surface area, particle size, and pore size distribution of Pakistani Ca-bentonite. *Arab. J. Geosci.*, 11, 15, 399.
- TOMBACZ, E. & SZEKERES, M., 2004: Colloidal behavior of aqueous montmorillonite suspensions: the specific role of pH in the presence of indifferent electrolytes. *Appl. Clay Sci.*, 27, 1–2, 75–94.
- TOMIĆ, M., DUNJIĆ, B., NIKOLIĆ, M. S., MALETAŠKIĆ, J., PAVLOVIĆ, V. B., BAJAT, J. & DJONLAGIĆ, J., 2018: Dispersion efficiency of montmorillonites in epoxy nanocomposites using solution intercalation and direct mixing methods. *Appl. Clay Sci.*, 154, 52–63.
- UDDIN, M. K., 2017: A review on the adsorption of heavy metals by clay minerals, with special focus on the past decade. *Chem. Eng. J.*, 308, 438–462.
- VACULÍKOVÁ, L., PLEVOVÁ, E. & RITZ, M., 2019: Characterization of montmorillonites by infrared and Raman spectroscopy for preparation of polymer-clay nanocomposites. *J. Nanosci. Nanotechnol.*, 19, 5, 2775–2781.
- WIESS, Z. & KUŽVART, M., 2005: Jílové minerály – jejich struktura a použití. *Praha, Karolinum*.

## Charakteristika jemnozrnnej frakcie montmorillonitu na prípravu polymérových ílovitých nanokompozitov

Cieľom štúdia bola detailná charakterizácia ílových minerálov (pred ich chemickou aktiváciou a po nej) na prípravu nanokompozitov polymér-íl v porovnaní s prírodným neupraveným materiálom. Komplexná štruktúrna charakterizácia jemnozrnných frakcií prispieva k lepšiemu pochopeniu fyzikálno-chemických vlastností a správania ílových minerálov a umožňuje plne využiť ich potenciál pri príprave ílových nanokompozitov s vyššími úžitkovými vlastnosťami na budúce priemyselné aplikácie.

Vzorky montmorillonitu sú charakteristické časticami spojenými do agregátov až do veľkosti niekoľkých desiatok mikrometrov. Natriifikácia má na montmorillonit dispergačný účinok, čím sa dosiahne zjemnenie zrna. Väzby v štruktúre montmorillonitu sú ovplyvnené najmä prítomnosťou molekúl vody. Absorpcia vody priamo súvisí s prítomnosťou dvoch najbežnejších katiónov,  $\text{Na}^+$  a  $\text{Ca}^{2+}$ , v medzivrstvovom priestore. Dvojmocné katióny  $\text{Ca}^{2+}$  udržujú štruktúrne vrstvy stabilnejšie a kompaktnejšie ako ich monovalentné ( $\text{Na}^+$ ) ióny. Po vstupe katiónov  $\text{Na}^+$  do štruktúry smektitu (montmorillonitu) slabšie väzby v rámci štruktúrnych vrstiev umožňujú molekulám vody (ale aj iným cudzím katiónom alebo molekulám) ľahší prístup k vrstvenej štruktúre. Radikálne zvýšenie objemu medzivrsty (až 10-násobne) ovplyvní katiónovú výmennú kapacitu montmorillonitu. Tento jav spolu so zväčšením objemu vedie k zväčšeniu špecifického povrchu a k zmenám adsorpčných vlastností montmorillonitu.

Boli použité štyri vzorky ílového minerálu montmorillonitu: SWy-2, SAz-2, STx-1b a Kunipia-F. Vzorky SAz-2 a STx-1b obsahujú katióny  $\text{Ca}^{2+}$  v medzivrstve, vzorka SWy-2 katióny  $\text{Na}^+$  aj  $\text{Ca}^{2+}$  a Kunipia-F iba katióny  $\text{Na}^+$ . Montmorillonity v prírodnom stave boli purifikované sedimentáciou podľa Stokesovho zákona (získaná jemná frakcia, veľkosť častíc < 5  $\mu\text{m}$ ). Na zlepšenie povrchových vlastností jemnozrnných frakcií sa urobila monoiónová chemická aktivácia vzoriek montmorillonitov obsahujúcich vápník v medzivrstve (SAz-2, STx-1b a SWy-2). Aktivované vzorky boli pripravené saturáciou 0,5 M vodným roztokom  $\text{Na}_2\text{CO}_3$  intenzívnym trepaním počas 24 hodín, oddelením zmesi centrifugáciou, následným premývaním destilovanou vodou a sušením pri 100 °C počas 24 hodín. Následne sa vykonala fyzikálno-chemická charakterizácia získaných materiálov, ako aj vstupných vzoriek metódami rtg. práškovej difrakcie, infračervenej spektroskopie, termickej analýzy, SEM analýzy a analýzy povrchu pomocou sorpcie plynov.

Röntgenová prášková difrakcia potvrdila prítomnosť montmorillonitu ako dominantnú minerálnu fázu a preukázala štruktúrne zmeny aktivovaných vzoriek, ktoré

ovplyvnili posun hlavnej bazálnej difrakcie montmorillonitu (001) na osi x doprava. Tento jav bol spôsobený výmenou katiónov medzi  $\text{Ca}^{2+}$  a  $\text{Na}^+$  z medzivrstvového priestoru montmorillonitovej štruktúry.

Infračervená spektroskopia charakterizovala absorpcné pásy pozorované v infračervených spektrách pôvodných foriem montmorillonitu. Jednotlivé typy montmorillonitov sa líšia typom minerálnych prímesí aj svojím chemickým zložením. Montmorillonit SAz-2 predstavoval takmer čistú vzorku. Iba nepatrý pás nachádzajúci sa v blízkosti 789  $\text{cm}^{-1}$  indikoval stopy amorfného oxidu kremičitého. Prímes kremeňa sa potvrdila dubletom pásov v oblasti vlnovej dĺžky 798 a 779  $\text{cm}^{-1}$  vo vzorkách SWy-2 a Kunipia-F. Vzorka STx-1b obsahovala prímes cristobalitu (794  $\text{cm}^{-1}$ ). Absorpčný pás pri vlnovej dĺžke 884  $\text{cm}^{-1}$  vo vzorke SWy-2 potvrdil prítomnosť Fe v oktaédrickej štruktúre tohto ílového minerálu. Po chemickej aktivácii sa vo všetkých infračervených spektrách použitých montmorillonitov zistili typické karbonátové pásy (1 430 a 880  $\text{cm}^{-1}$ ). Súčasne bola pozorovaná zmena polohy pásu zodpovedajúceho vibráciám povrchovo viazanej vody. Pás sa posúva k vyšším vlnovým dĺžkam.

Pri hodnotení tepelnej stability jemnozrnných frakcií montmorillonitov a ich aktivovaných sodných foriem si multánnou termogravimetriou a diferenčnou termickou analýzou mali študované vzorky rovnaký trend. Teplotné krivky vykazovali dva teplotné intervale. Prvý interval (100 – 300 °C) zodpovedá uvoľňovaniu adsorbovanej vody z medzivrsty. Druhý interval (500 – 1 100 °C) predstavuje uvoľňovanie hydroxylových skupín a následné fázové premeny. Zdvojený pík na DTA krivke zodpovedajúci strate adsorbovanej vody je spojený s Ca formou montmorillonitov. Po aktiváčnom procese bol získaný jednostupňový pík, typický pre Na montmorillonitovú formu. Teplota fázovej premeny sa pri vzorke STx-1b zvýšila, zatiaľ čo pri vzorkách SWy-2 a SAz-2 fázová premena nebola pozorovaná.

Podrobnej analýzy adsorpčných izoteriem sa uskutočnili na porovnanie povrchových vlastností študovaných vzoriek. Namerané izotermy všetkých vzoriek montmorillonitov ukázali hysteréznu slučku medzi adsorpčnými a desorpčnými vettami izoteriem. Adsorpčné izotermy SWy-2, SAz-2 a Kunipia-F boli veľmi podobné, pomalé zvyšovanie objemu adsorbovaného plynu v celom rozsahu relatívneho tlaku s prudkým nárastom pri  $p/p_0 \approx 0,95$  bolo spojené s prítomnosťou väčších pórov, makropórov. Hysterézne slučky vzoriek SWy-2, STx-1b a Kunipia-F korešpondujú s typom H3 potvrdzujúcim prítomnosť pórov typických pre hlinitokremičitanové materiály.

Slučka vzorky SAz-2 je typu H4, spojená s prítomnosťou štrbinovitých pórov, ale počiatočná časť izotermy je spojená s prítomnosťou mikropórov. Najvyššia hodnota špecifického povrchu bola v prípade vzorky STx-lb (99,4 m<sup>2</sup>/g).

Zmeny vlastností po modifikácii vzoriek montmorillonitov boli pozorované aj z distribučných kriviek diferenciálnej veľkosti pórov odvodnených z desorpčných vetiev izoteriem. Vzorka SWy-2 vykázala širšiu distribúciu, v rozsahu od 4,3 do 44,7 nm s maximom  $R_{\max} = 9,8$  nm (polomer pórov). Zodpovedá to prítomnosti mezo- a makropórov. Ostré maximum polomeru pórov pri  $R \approx 1,9$  nm zodpovedá skoku na desorpčnej izoterme, ktorý sa nazýva vynútené uzavretie hysteréznej slučky a nezodpovedá skutočnému pórom. Toto maximum možno pozorovať pri všetkých študovaných vzorkách. Vzorky SAz-2 a NaSAz-2 majú veľmi podobné distribučné krivky, mierny rozdiel možno pozorovať iba v rozsahu veľkých mezopórov a makropórov. Môže to byť spojené s nižšou hodnotou objemu adsorbovaného plynu na adsorpčnej izoterme. Vzorka

SAz-2 bola mikroporéznejšia a modifikácia významne neovplyvnila jej textúrne vlastnosti. Vzorka STx-lb neobsahovala mikropóry, bola hľavne mezoporézno-makroporézna, s vyšším obsahom väčších mezopórov ( $R_{\max} = 21,6$  nm). Po modifikácii vzorky sa pozoroval posun distribučnej krivky doľava k hodnotám nižších mezopórov ( $R_{\max} = 3,05$  nm). Táto skutočnosť zodpovedá zníženiu hodnoty celkového objemu pórov. Vzorka Kunipia-F vykázala širokú distribúciu, od 3,03 do 143,3 nm s dvomi maximami,  $R_{\max 1} = 15,7$  nm a  $R_{\max 2} = 46,5$  nm. Potvrdilo to prevažne mezoporézny charakter s malou hodnotou špecifického povrchu. Získané jemné frakcie montmorillonitu majú potenciál byť vhodným materiálom na prípravu ílových nanokompozitov s lepšími sorpčnými vlastnosťami využiteľnými v environmentálnych oblastiach.

Doručené / Received: 19. 5. 2022  
Prijaté na publikovanie / Accepted: 21. 6. 2022